Breaking up CO_2 through pressure-induced redox reaction with rhenium

Dylan Durkee[1,2] and S. X. Hu[1,2,3,*]

[1]*Laboratory for Laser Energetics, University of Rochester, Rochester, New York 14623, USA*
[2]*Department of Physics and Astronomy, University of Rochester, Rochester, New York 14627, USA*
[3]*Department of Mechanical Engineering, University of Rochester, Rochester, New York 14627, USA*

(Received 18 August 2023; revised 19 October 2023; accepted 18 December 2023; published 11 January 2024)

We present results from density-functional theory-based molecular dynamics simulations of fluid mixtures of carbon dioxide (CO_2) and rhenium (Re) metal at pressures up to 45 GPa and a temperature of 4000 K. Covalently bonded carbon chains form as a result of a redox reaction between CO_2 and Re, whereas a pure CO_2 fluid is stable against decomposition at the same conditions. These findings have implications in reducing CO_2 by pressure-induced redox reactions with transition metals, which may play a role in CO_2 destruction and carbon storage as related to possible solutions to the current climate crisis.

DOI: 10.1103/PhysRevB.109.014207

I. INTRODUCTION

Over the last several decades, there has been an extensive amount of research on the carbon dioxide (CO_2) system at high pressures and temperatures. Static high-pressure experiments using diamond-anvil cells (DACs) have reported numerous molecular and nonmolecular phases of CO_2 at gigapascal (GPa) pressures [1–4], and the melting line has also been measured up to 35 GPa [5–7]. In conjunction with theoretical efforts [8–10] the CO_2 phase diagram has been constructed at pressure-temperature (*P-T*) conditions of the Earth's mantle (i.e., up to 120 GPa and ~4000 K) and beyond. Additionally, there has been an abundance of experimental and theoretical research on the dynamic behavior of CO_2 at ultrahigh pressures up to 1 TPa, including its optical and transport properties, its stability as a liquid, and its equation of state [11–16].

Early experimental reports suggested that CO_2 reduces to diamond and high-pressure $\varepsilon{-}O_2$ via decomposition at pressures greater than ~ 30 GPa and temperatures greater than ~ 1700 K [7,17]. Moreover, early theoretical work predicted that CO_2 would decompose at multimegabar pressures [18]. However, more recent experiments have shown CO_2 to be remarkably stable at these *P-T* conditions, and several theoretical predictions support the stability of CO_2 against decomposition to pressures greater than 140 GPa and temperatures up to 10 000 K [8,9,19–21]. Therefore, CO_2 may exist at *P-T* conditions relevant to the Earth's geotherm. In fact, CO_2 may result from reactions between SiO_2 and carbonates such as $MgCO_3$ or $CaCO_3$ [22], as well as from decomposition of calcite ($CaCO_3$) at high temperatures due to shock impacts [23]. At higher pressures between 200 and 900 GPa, a layered structure (with space group $P42/nmc$) in which carbon exhibits tetrahedral coordination is predicted to be thermodynamically stable [24].

Recent experiments using laser-heated DACs explored possible chemical reactions between several transition metals (Au, Pt, and Re) and CO_2 [25,26]. Rhenium (Re) was reported to react with CO_2, reducing it to either diamond or graphite at pressures between 8–48 GPa and $T > 1500$ K and forming ReO_2 as evidenced by x-ray diffraction. ReO_2 was also detected as a contaminant in another recent DAC study which used Re gasket material, after laser heating CO_2 at 34 GPa [21]. Pressure-induced redox reactions between CO_2 and transition metals like Re may present a unique mechanism for the reduction of CO_2 to elemental carbon and storing it in solid form. Such high-pressure reactions involving CO_2 are relatively unexplored, even though some preliminary experiments involving surface reactions exist. Understanding these high-pressure reactions also has relevance to topics such as diamond formation and the relative stability of carbon-bearing compounds at planetary mantle conditions.

In this work, we use *ab initio* molecular dynamics (AIMD) to simulate the pressure-induced redox reaction in CO_2 and Re fluid mixtures at a temperature of 4000 K and at pressures varying from ~ 0.3 up to 45 GPa. Our simulations explore the complex liquid structure and different chemical species that form in the reaction. The roles that Re and high pressures play in facilitating the reduction of CO_2 are discussed.

II. METHODS

The AIMD simulations were performed using the Vienna *ab initio* Simulation Package (VASP) [27–30] software. The exchange-correlation functional used for all calculations was the Perdew-Burke-Ernzerhof in the generalized gradient approximation [31]. For all calculations, we use projector augmented-wave (PAW) pseudopotentials (PPs) with 4- and 6 electrons for carbon and oxygen, respectively, and 7-electron PAW PPs for Re [32]. We chose a cutoff energy of 910 eV with the Γ-point sampling for all CO_2 + Re simulations. Separate simulations containing 128, 288, and 768 total atoms were performed, each simulation with a 1:1 ratio between CO_2

*shu@lle.rochester.edu

molecule to Re atom. Convergence tests for energy cutoff and system-size effects can be found in the Supplemental Material [33] (see also Refs. [38–42] therein).

To set up the $CO_2 + Re$ fluid simulations, we began with a solid system of phase I *Pa*-3 [1] CO_2 and allowed that pure CO_2 system to melt and equilibrate at $T = 4000$ K (2-4-ps equilibration time) before randomly adding Re atoms to the CO_2 fluid mixture and simulating the $CO_2 + Re$ fluid mixture for 6-10 ps. Re atoms were added at randomly generated positions of the simulation cell of the pure CO_2 fluid which was equilibrated at 4000 K, where the minimum nearest neighbor of each Re atom was constrained to a distance of 1.8–1.9 Å. Nearest-neighbor distances larger than 1.9 Å were not feasible under these density conditions of the simulation cells. In addition to the "fluid-mixture" picture, we have also performed simulations with a different scenario: we start with solid phase-I CO_2, add Re atoms into the interstitial sites, melt the solid mixture, and equilibrate the resulting fluid mixture at 4000 K. These simulations yielded very similar results (see Supplemental Material [33]) in the $g(r)$ and species-count analysis as our fluid-mixture simulations. All simulations were performed in the *NVT* ensemble using the Nosé-Hoover thermostat [34,35] for temperature control, with a time step of 1.5 fs.

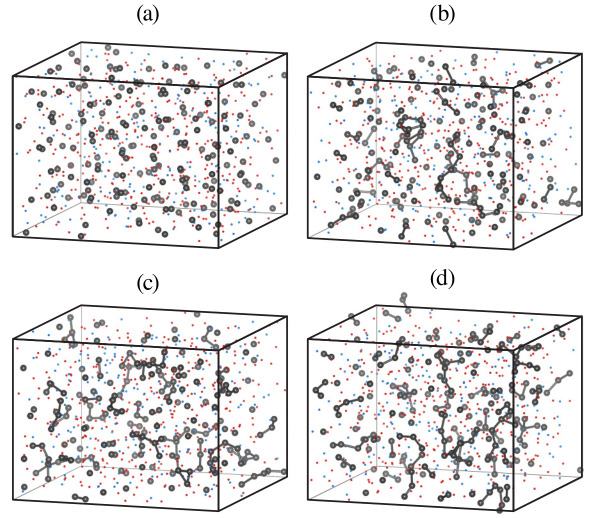

FIG. 1. Snapshots of the $CO_2 + Re$ fluid reaction at 45 GPa (corresponding initial density of 10.53 g/cc) and 4000 K from the AIMD simulation at times (a) 0 ps, (b) 0.75 ps, (c) 2 ps, and (d) 7 ps, with emphasis on C–C bonding formation. C atoms are colored gray, along with C–C bonds depicted in (b), (c), and (d). Re and O atoms are colored blue and red, respectively. The system size is 768 total atoms with an initial 192 CO_2 molecules and 192 Re atoms.

III. RESULTS

Simulations were done at a temperature of $T = 4000$ K for $CO_2 + Re$ fluid mixtures at three different pressures: $P < 1$ GPa (1.53 g/cc), $P = 20$ GPa (8.45 g/cc), and $P = 45$ GPa (10.53 g/cc). In this pressure range, the chosen temperature of 4000 K is above the measured melt line of Re according to DAC experiments [36] and near a theoretically predicted melt curve [37] at the highest simulation pressure of 45 GPa. The fluid behavior of Re in our simulations is seen at the highest pressure of 45 GPa according to the mean-squared displacement analysis shown in Fig. S1 in the Supplemental Material [33]. Snapshots along the AIMD trajectory for a system of 192 CO_2 molecules and 192 Re atoms in a fluid mixture at 45 GPa are shown in Fig. 1 (generated with VESTA software [43]), where we emphasize the dynamics of the C atoms throughout the simulation. At time $t = 0$ ps in Fig. 1(a), Re atoms (shown as small blue spheres) are randomly distributed in the CO_2 fluid, and the C atoms (larger gray spheres) are bound to their respective O atoms (small red spheres) as CO_2 molecules. As the simulation progresses in time [Figs. 1(b)–1(d)], the CO_2 molecules are broken up by reaction with the Re atoms. As a result, the free C atoms in the system begin to bond with each other. C-C chains form in the simulation [Fig. 1(b)], and the average number of C-C chains drastically increase within the first couple of picoseconds as seen in the similar distribution of C-C chains in Figs. 1(c) and 1(d).

Radial distribution functions, $g(r)$, provide information about structural correlations between atoms inside a liquid, solid, or gas system. The $g(r)$ curves (see Supplemental Material [33] for more information of $g(r)$ construction) from simulations at 45 GPa and 4000 K for the three main atom pairs of interest, C-C, C-O, and Re-O, are plotted in Fig. 2 as a function of radial distance at different times along the AIMD trajectory. Behavior typical of a liquid system is seen in these $g(r)$ curves where the peaks represent short-range bonding or structure in the first coordination spheres of the atom pairs. At $t = 0.15$ ps (shown by the red curves), the contribution of the intramolecular C–O bond distance dominates the C-O $g(r)$, and the C-C $g(r)$ already shows a small peak forming at a radial distance of ~ 1.45 Å. The C-O peak represents the initial CO_2 molecules in the system at the beginning

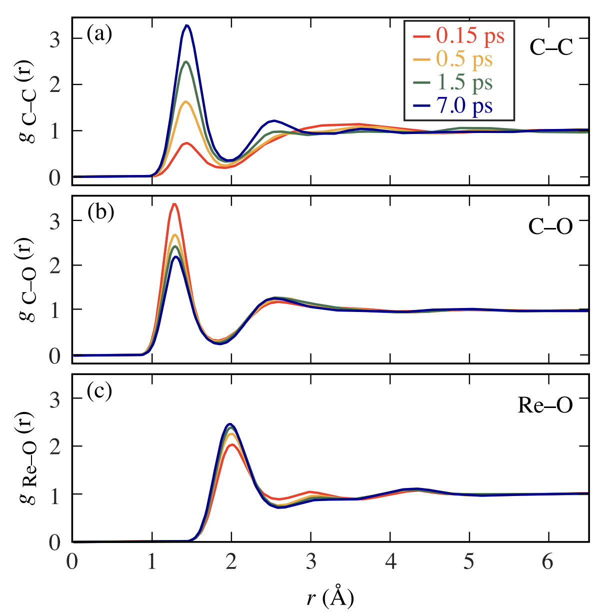

FIG. 2. Radial distribution functions $g(r)$ calculated for three atom-pairs: (a) C-C, (b) C-O, and (c) Re-O at different times across the 768-atom AIMD simulation at 45 GPa (10.53 g/cc) and 4000 K. Each curve represents the average $g(r)$ of a bin size of 200 AIMD steps around the labeled value.

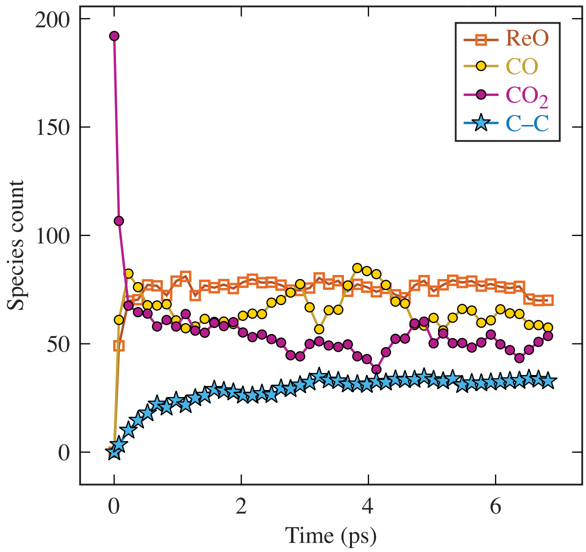

FIG. 3. The number of chemical species as a function of time across the AIMD simulation at 45 GPa (corresponding to 10.53 g/cc initial density) and 4000 K, for the main interactions of interest. Each data point represents an average species count over a bin size of 0.15 ps. The simulation starts with 192 CO_2 molecules and 192 Re atoms (768 total atoms), the same simulation as Figs. 1 and 2.

of the AIMD simulation. As the simulation progresses in time, the reaction between the CO_2 molecules and the Re atoms in the fluid mixture occurs quickly; the significant decrease in peak height indicates a reduction in the amount of C–O bonds as CO_2 reduces to CO and C species. The triple bond between C and O in CO should produce a shorter bond length than the double-bond CO_2; indeed, the bond lengths are ~ 1.12 and ~ 1.16 Å at ambient conditions for CO and CO_2, respectively. Thus, although a slight shift to lower radial distances in the first peak of the C-O $g(r)$ might be expected, such a shift was not observed. This is likely due to the broadness of the peak at the high temperature (4000 K) investigated here, combined with the fact that, at least at ambient conditions, the difference in bond length between the two carbon-oxide species is rather small. Accordingly, the first peak in the $g(r)$ of C-C at a radial distance of around ~ 1.45 Å increases in height over the first several picoseconds of the simulation, indicating an increase of bonding between free C atoms in the system. The height of this $g(r)$ peak eventually saturates and fluctuates around a constant. The high pressure allows the randomly placed Re atoms to be in favorable proximity to the CO_2 molecules. As a result, the Re atoms almost immediately interact with the O atoms of nearby CO_2 molecules. The initial Re-O distances in the simulations are similar in value to Re–O bond distances at ambient pressure for example, where the Re–O bond distances typical of Re-oxides range between $\sim$1.6 and 2.2 Å [44–46].

Next, we discuss results of a geometric analysis to count the relative amounts of chemical species present in the liquid mixture throughout the simulation. Boates *et al.,* for example, used a similar molecular fraction analysis looking at the structure of liquid CO_2 [12] at high pressures and temperatures. The "species count" analysis performed here counts the number of secondary atoms in an atom pair within a sphere centered on the reference atom. For example, for the Re-O atom pair, a sphere of a specified cutoff radius R_{cut} is centered on each reference Re atom, and the number of secondary atoms (O atoms in this example) are counted. The number of occurrences of each species detected (ReO, CO, CO_2, C-C, etc.) is determined for each individual time step along the AIMD trajectory. More information on the species-count procedure can be found in the Supplemental Material [33].

The results of this species-count analysis for the simulation at 45 GPa are shown in Fig. 3, where we plot the main species of interest as a function of simulation time. At $t = 0$ ps, only the total 192 CO_2 molecules are detected, and the number of detected CO_2 molecules decreases rapidly in the first picosecond of the simulation, accompanied by a relative increase in the count of CO and ReO species. Additionally, the reduction of CO_2 to free C atoms results in a gradual increase in C–C bonding and thus the number of detected C-C interactions shown by the stars in Fig. 3. Longer simulation times, perhaps tens or hundreds of picoseconds, could potentially help determine whether the amount of CO and

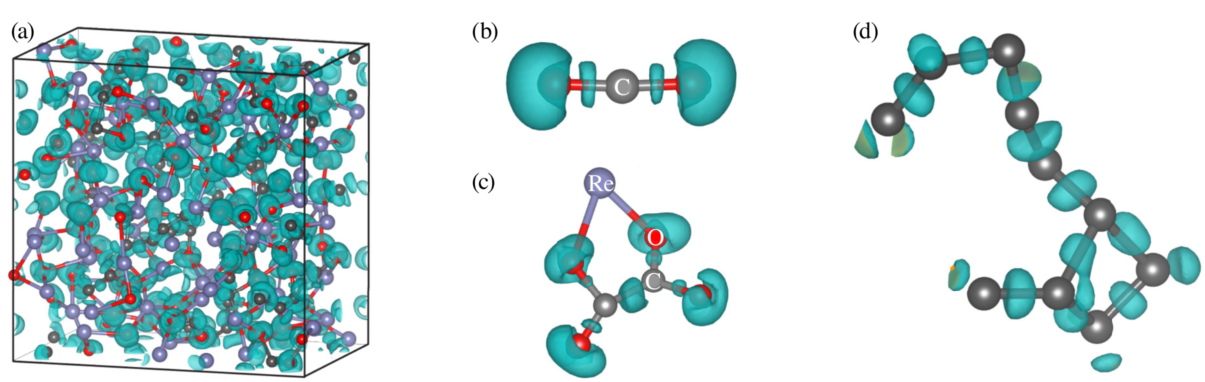

FIG. 4. Isosurfaces of calculated electron localization functions (ELFs) for (a) the entire simulation cell of 288 atoms at $t = 3$ ps, (b) an isolated CO_2 molecule in a simulation of a pure CO_2 fluid of 64 atoms, (c) an isolated interaction between Re and CO_2 molecules within the CO_2 + Re fluid reaction 288-atom simulation, and (d) an isolated chain of C atoms at one step during the CO_2 + Re fluid 288-atom simulation, showing the covalent bonds between the C atoms. C atoms are shown in gray; Re and O atoms are shown in blue and red, respectively. The isosurfaces represent ELF values of 0.81 (a), (c), and (d), and 0.8 (b). The initial densities of the systems for the ELF calculations shown in (a)–(d), respectively, are 10.53 g/cc (45 GPa), 1.62 g/cc (4 GPa), 8.45 g/cc (20 GPa), and 10.53 g/cc (45 GPa).

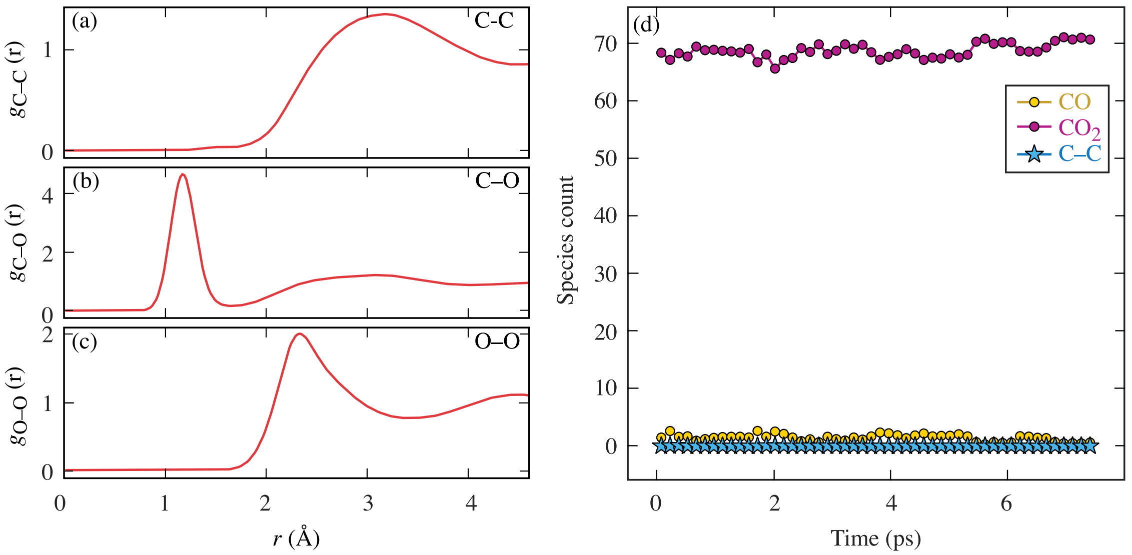

FIG. 5. Radial distribution functions $g(r)$ for (a) C-C, (b) C-O, and (c) O-O atom pairs for a pure CO_2 fluid simulation of 72 CO_2 molecules at an average pressure of ~45 GPa (2.90 g/cc) and at 4000 K. The $g(r)$ curves represent an average over 2000 AIMD steps centered at 6 ps, so the system has had sufficient time to equilibrate. (d) Number of species as a function of simulation time for the same pure CO_2 fluid simulation. Each data point represents an average number of chemical species in bins of size 0.15 ps. A $1 \times 1 \times 1$ k-point grid was used for this simulation, and the simulation began with solid phase I CO_2 at 300 K, the temperature was ramped up to 4000 K over 1 ps, and then the system was equilibrated at 4000 K for 7.5 ps.

ReO species in the system would fully reduce and oxidize, respectively, to produce more C-C interactions and the higher stoichiometric Re oxides ReO_2 and ReO_3. However, it is unknown whether the $CO_2 + Re$ fluid mixture energetically favors Re-carbide or Re-oxide formation at the studied pressures (20 and 45 GPa) and temperature (4000 K). See Figs. S2 and S3 in the Supplemental Material [33] for $g(r)$ and species-count results for other atom pairs not evaluated in the main text. The $g(r)$ and species-count analysis of a $CO_2 + Re$ fluid simulation at 20 GPa and 4000 K shows similar results as the simulations at 45 GPa shown in Figs. 1 –3; the 20-GPa analysis is shown in Figs. S4 and S5 in the Supplemental Material [33].

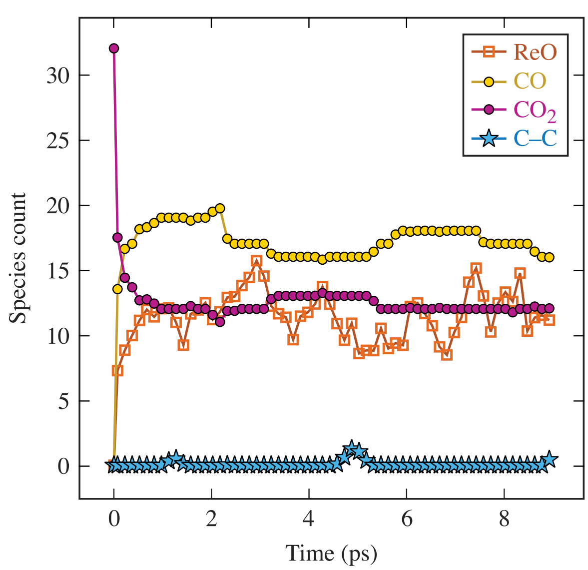

FIG. 6. Number of species as a function of simulation time in a $CO_2 + Re$ fluid mixture simulation of 128 total atoms, at low pressure of < 1 GPa and at 4000 K. The initial density of the system is 1.53 g/cc. Although Re-O interactions are apparent from this analysis, there is a clear lack of C-C interactions throughout the entire simulation.

Electron localization functions (ELFs) were calculated in the VASP software at selected steps along AIMD trajectories. The individual molecules and clusters depicted in Figs. 4(b)–4(d) were isolated from these system calculations. The complexity of the $CO_2 + Re$ liquid structure at high pressure and temperature can be seen in the ELF of the simulation cell shown in Fig. 4, where isosurfaces are shown for a value of the ELF$[n(r)] \sim 0.8$. In general, ELF values above 0.7 indicate that electrons are localized due to, i.e., nuclei, bonding, or lone pairs [47]. Many different transient interactions between Re, C, and O atoms are observed throughout the simulation. In a pure CO_2 fluid at these conditions, the CO_2 molecule is stable against decomposition, and its ELF is shown in Fig. 4(b), where the electrons are confined to the C–O bonds. Figure 4(c) shows an example where a Re atom interacts with two adjacent CO_2 molecules, allowing for some electron localization between the two C atoms. The covalent nature of the C–C bonding is emphasized by the ELF isosurfaces of the C-C chains shown in Fig. 4(d), where electron localization on the bonds between C atoms are shown by the isosurfaces, and some of the C atoms also exhibit lone-pair lobes.

Next, it is important to note that CO_2 does not significantly reduce in simulations of a pure CO_2 fluid at the same P-T conditions of 45 and 20 GPa, and 4000 K. This is consistent with recent literature that suggests CO_2 is stable against decomposition at these conditions [8,20], and therefore in the pure CO_2 fluid simulation, C–C bonding does not occur. The radial distribution function and species analysis for the pure CO_2

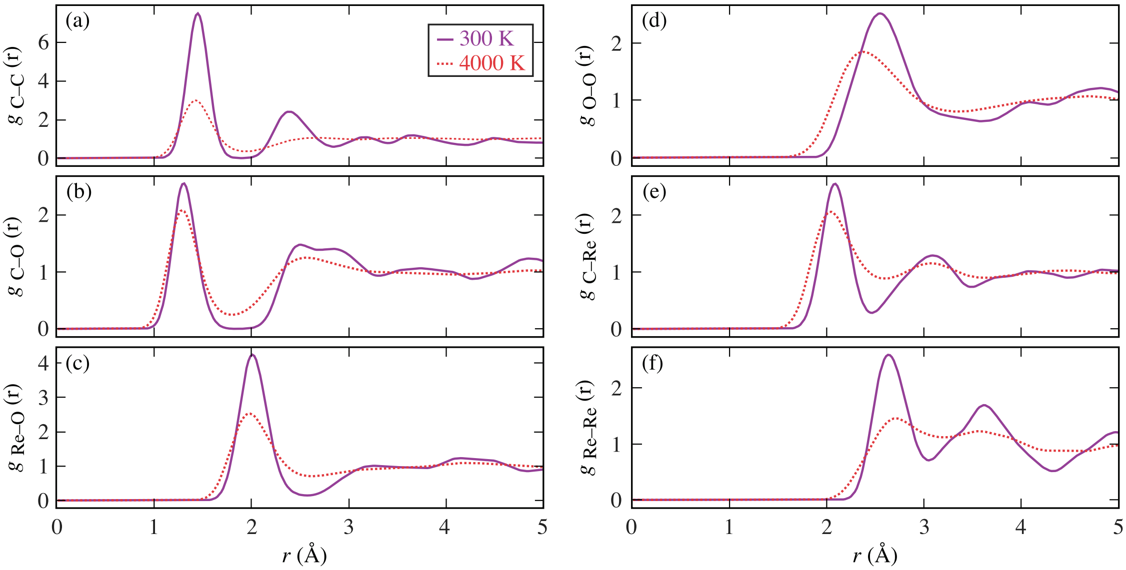

FIG. 7. Radial distribution functions, $g(r)$, calculated from a 128-atom AIMD simulation with a 1:1 ratio of CO_2 molecules to Re atoms at 45 GPa (10.53 g/cc), for (a) C-C, (b) C-O, (c) Re-O, (d) O-O, (e) C-Re, and (f) Re-Re atom pairs at 4000 K before quenching (red/dotted), and 300 K after equilibrating for 15 ps (purple/solid). After the system was adequately equilibrated at T = 4000 K for 9 ps, the temperature was quenched from 4000 down to 300 K over a period of 60 ps. Then, the system was equilibrated at 300 K for an additional 15 ps. The $g(r)$ curves at 4000 K (red/dotted) are averaged over the final 3 ps of the equilibration period (9 ps total), i.e., 2000 MD steps, while the $g(r)$ curves at 300 K are averaged over the final 4.5 ps of the equilibration period (15 ps), or 3000 MD steps.

fluid, shown in Fig. 5, verify the stability of the CO_2 molecule at these conditions. Thus, we can rule out the reduction of CO_2 through high pressure and temperature application alone and conclude that redox chemistry involving Re facilitates this reduction.

Interestingly, Re-O interactions are still observed in an AIMD simulation at less than 1 GPa and 4000 K as seen by the species-count curves in Fig. 6. A significant decrease in the fraction of CO_2 is seen in this analysis, accompanied by an increase in Re-O interactions. A comparatively greater amount of CO species is observed than those of high-pressure (20 and 45 GPa) simulations. Despite the presence of Re-O interactions and the reduction of CO_2, C–C bonded species are not detected in any significant amount in the $<$ 1-GPa simulation. Thus, these observations indicate that higher pressures ($>$ 1 GPa) are required for C–C bonding to occur following the reduction of CO_2 by the Re atoms.

Finally, after allowing $CO_2 + Re$ fluid mixture to equilibrate at 4000 K, we also simulated a temperature quench from T = 4000 to 300 K, resulting in a pressure decrease from $\sim$ 45 to 25 GPa (Fig. 7). The total quenching time was 60 ps on a 128-atom system, with an additional 15-ps equilibration period at the final temperature of 300 K. The size of the system is too small to resolve nucleation of C-C chains into the expected diamond structure. However, the $g(r)$ analysis for the quenched system shows that the C–C bonding persists. These results suggest that the redox reaction between CO_2 and Re is irreversible when the temperature is quenched to room temperature. Interestingly, surface reactions of CO_2 and Re gaskets in DAC experiments [21,25] also found the redox reaction irreversible on both temperature and pressure quench. Coordination of the bonded C atoms in the final quenched structure (see Fig. S10 [33]) show two- and threefold coordination, but no atoms display fourfold coordination as in face-centered cubic (FCC) diamond. Since AIMD simulations are limited to small system sizes typically less than 1000 atoms, they are not ideal in capturing the possible nucleation of the diamond structure that may result from the $CO_2 + Re$ redox reaction. Nucleation may possibly be observed by using machine-learning interatomic potentials (MLPs). For example, MLPs have recently been used to generate large-scale atomistic simulations ($>$200000 atoms) of shock-compressed FCC, in which BC8 diamond nucleation was observed [48]. The possibility of simulating diamond nucleation resulting from the $CO_2 + Re$ (or other transition metal) redox reactions is a point of future investigation.

IV. SUMMARY

In summary, AIMD simulations based on density-functional theory (DFT have been performed in a range of pressures up to 45 GPa and at a temperature of 4000 K on $CO_2 + Re$ fluid mixtures. These simulations reveal a rich and complex chemistry in these fluid mixtures where strong Re-O interactions result in the reduction of CO_2 to elemental carbon which allows for covalent C–C bonding. A secondary material with the role of a reducing agent is necessary to break up the CO_2 molecules and allow for free C atoms to form bonds, whereas in a pure CO_2 fluid the CO_2 molecules are remarkably stable against decomposition at the conditions studied here. The reduction of CO_2 molecules readily occurs at pressures of 20 and 45 GPa. Low-pressure ($\sim$ 0.3 GPa) simulations also show Re and CO_2 interactions, although the amount of free C atoms in the system is significantly smaller and no notable C–C bonding is observed.

Diamond is expected to be the stable form of carbon at these P-T conditions; however, the system sizes (maximum 768 atoms) affordable in the current DFT-based simulations limit our ability to observe bulk diamond formation. Although ELF is used to analyze bonding between C atoms, this analysis also does not capture whether graphite or diamond formation will be favored. Future work will address the form of the resulting solid carbons in such redox reactions. Importantly, high-pressure redox reactions between CO_2 and other transition metals represent an underexplored area of research. Such investigations into high-pressure induced redox chemistry have relevance to the relative stability of carbon-bearing compounds (CO_2 and carbides like ReC, SiC, FeC, etc.) and carbon-bearing minerals ($MgCO_3$, $FeCO_3$, $CaCO_3$, etc.) in planetary interiors [3]. Finally, the $CO_2 + Re$ redox system at high pressures and temperatures presents a route to CO_2 reduction to solid carbon and justifies further research into the potential application of high-pressure mediated redox reactions in CO_2 systems to carbon capture and storage technologies, which could potentially help in finding viable solutions to the urgent climate crisis.

ACKNOWLEDGMENTS

This work is supported by NSF Physics Frontier Center Award No. PHY-2020249 and Department of Energy National Nuclear Security Administration under Award No. DE-NA0003856.

[1] K. Aoki, H. Yamawaki, M. Sakashita, Y. Gotoh, and K. Takemura, Crystal structure of the high-pressure phase of solid CO_2, Science **263**, 356 (1994).

[2] C.-S. Yoo, Physical and chemical transformations of highly compressed carbon dioxide at bond energies, Phys. Chem. Chem. Phys. **15**, 7949 (2013).

[3] C.-S. Yoo, *Carbon Redox Chemistry: Deep Carbon Dioxide and Carbonates in Carbon in Earth's Interior*, edited by C. E. Manning, J.-F. Lin, and W. L. Mao (American Geophysical Union, Washington, D.C., 2020), pp. 67–75.

[4] M. Santoro, F. A. Gorelli, K. Dziubek, D. Scelta, and R. Bini, *Structural and Chemical Modifications of Carbon Dioxide on Transport to the Deep Earth in Carbon in Earth's Interior*, edited by C. E. Manning, J.-F. Lin, W. L. Mao (American Geophysical Union, Washington, D.C. 2020), pp. 55–65.

[5] V. M. Giordano, F. Datchi, and A. Dewaele, Melting curve and fluid equation of state of carbon dioxide at high pressure and high temperature, J. Chem. Phys. **125**, 054504 (2006).

[6] V. M. Giordano and F. Datchi, Molecular carbon dioxide at high pressure and high temperature, Europhys. Lett. **77**, 46002 (2007).

[7] K. D. Litasov, A. F. Goncharov, and R. J. Hemley, Crossover from melting to dissociation of CO_2 under pressure: implications for the lower mantle, Earth Planet. Sci. Lett. **309**, 318 (2011).

[8] B. Boates, A. M. Teweldeberhan, and S. A. Bonev, Stability of dense liquid carbon dioxide, Proc. Natl. Acad. Sci. USA **109**, 14808 (2012).

[9] A. M. Teweldeberhan, B. Boates, and S. A. Bonev, CO_2 in the mantle: melting and solid–solid phase boundaries, Earth Planet. Sci. Lett. **373**, 228 (2013).

[10] B. H. Cogollo-Olivo, S. Biswas, S. Scandolo, and J. A. Montoya, *Ab initio* determination of the phase diagram of CO_2 at high pressures and temperatures, Phys. Rev. Lett. **124**, 095701 (2020).

[11] C. Wang and P. Zhang, Thermophysical properties of liquid carbon dioxide under shock compressions: quantum molecular dynamic simulations, J. Chem. Phys. **133**, 134503 (2010).

[12] B. Boates, S. Hamel, E. Schwegler, and S. A. Bonev, Structural and optical properties of liquid CO_2 for pressures up to 1 TPa, J. Chem. Phys. **134**, 064504 (2011).

[13] S. Root, K. R. Cochrane, J. H. Carpenter, and T. R. Mattsson, Carbon dioxide shock and reshock equation of state data to 8 Mbar: experiments and simulations, Phys. Rev. B **87**, 224102 (2013).

[14] C. J. Wu, D. A. Young, P. A. Sterne, and P. C. Myint, Equation of state for a chemically dissociative, polyatomic system: carbon dioxide, J. Chem. Phys. **151**, 224505 (2019).

[15] L. E. Crandall, J. R. Rygg, D. K. Spaulding, T. R. Boehly, S. Brygoo, P. M. Celliers, J. H. Eggert, D. E. Fratanduono, B. J. Henderson, M. F. Huff, R. Jeanloz, A. Lazicki, M. C. Marshall, D. N. Polsin, M. Zaghoo, M. Millot, and G. W. Collins, Equation of state of CO_2 shock compressed to 1 TPa, Phys. Rev. Lett. **125**, 165701 (2020).

[16] L. E. Crandall, J.R. Rygg, D. K. Spaulding, M. F. Huff, M. C. Marshall, D. N. Polsin, R. Jeanloz, T. R. Boehly, M. Zaghoo, B. J. Henderson, S. Brygoo, P. M. Celliers, J. H. Eggert, D. E. Fratanduono, A. Lazicki, M. Millot, and G. W. Collins, Equation-of-state, sound speed, and reshock of shock-compressed fluid carbon dioxide, Phys. Plasmas **28**, 022708 (2021).

[17] O. Tschauner, H. Mao, and R. J. Hemley, New transformations of CO_2 at high pressures and temperatures, Phys. Rev. Lett. **87**, 075701 (2001).

[18] S. Serra, C. Cavazzoni, G. L. Chiarotti, S. Scandolo, and E. Tosatti, Pressure-induced solid carbonates from molecular CO_2 by computer simulation, Science **284**, 788 (1999).

[19] K. F. Dziubek, M. Ende, D. Scelta, R. Bini, M. Mezouar, G. Garbarino, and R. Miletich, Crystalline polymeric carbon dioxide stable at megabar pressures, Nat. Commun. **9**, 3148 (2018).

[20] D. Scelta, K. F. Dziubek, M. Ende, R. Miletich, M. Mezouar, G. Garbarino, and R. Bini, Extending the stability field of polymeric carbon dioxide phase V beyond the earth's geotherm, Phys. Rev. Lett. **126**, 065701 (2021).

[21] A. F. Goncharov, E. Bykova, M. Bykov, E. Edmund, J. S. Smith, S. Chariton, and V. B. Prakapenka, Assessing the stability fields of molecular and polymeric CO_2, Phys. Rev. Mater. **7**, 053604 (2023).

[22] M. Moog, F. Pietrucci, and A. M. Saitta, Carbon dioxide under earth mantle conditions: from a molecular liquid through a reactive fluid to polymeric regimes, J. Phys. Chem. A **125**, 5863 (2021).

[23] Y. Umeda, K. Fukui, T. Sekine, M. Guarguaglini, A. Benuzzi-Mounaix, N. Kamimura, K. Katagiri, R. Kodama, T. Matsuoka, K. Miyanishi, A. Ravasio, T. Sano, and N. Ozaki, Hugoniot and released state of calcite above 200 GPa with implica-

tions for hypervelocity planetary impacts, Icarus **377**, 114901 (2022).

[24] M.-S. Lee, J. A. Montoya, and S. Scandolo, Thermodynamic stability of layered structures in compressed CO_2, Phys. Rev. B **79**, 144102 (2009).

[25] D. Santamaría-Pérez, C. McGuire, A. Makhluf, A. Kavner, R. Chuliá-Jordán, J. Pellicer-Porres, D. Martinez-García, A. Doran, M. Kunz, P. Rodríguez-Hernández *et al.*, Exploring the chemical reactivity between carbon dioxide and three transition metals (Au, Pt, and Re) at high-pressure, high-temperature conditions, Inorg. Chem. **55**, 10793 (2016).

[26] R. Chuliá-Jordán, D. Santamaría-Pérez, T. Marqueño, J. Ruiz-Fuertes, and D. Daisenberger, Oxidation of high yield strength metals tungsten and rhenium in high-pressure high-temperature experiments of carbon dioxide and carbonates, Cryst. **9**, 676 (2019).

[27] G. Kresse and J. Hafner, *Ab initio* molecular dynamics for liquid metals, Phys. Rev. B **47**, 558 (1993).

[28] G. Kresse and J. Hafner, *Ab initio* molecular-dynamics simulation of the liquid-metal–amorphous-semiconductor transition in germanium, Phys. Rev. B **49**, 14251 (1994).

[29] G. Kresse and J. Furthmüller, Efficiency of *ab-initio* total energy calculations for metals and semiconductors using a plane-wave basis set, Comput. Mater. Sci. **6**, 15 (1996).

[30] G. Kresse and J. Furthmüller, Efficient iterative schemes for *ab initio* total-energy calculations using a plane-wave basis set, Phys. Rev. B **54**, 11169 (1996).

[31] J. P. Perdew, K. Burke, and Y. Wang, Generalized gradient approximation for the exchange-correlation hole of a many-electron system, Phys. Rev. B **54**, 16533 (1996).

[32] G. Kresse and D. Joubert, From ultrasoft pseudopotentials to the projector augmented-wave method, Phys. Rev. B **59**, 1758 (1999).

[33] See Supplemental Material at http://link.aps.org/supplemental/10.1103/PhysRevB.109.014207 for more information on computational analysis, which includes Refs. [37–41].

[34] S. Nosé, A unified formulation of the constant temperature molecular dynamics methods, J. Chem. Phys. **81**, 511 (1984).

[35] W. G. Hoover, Canonical dynamics: equilibrium phase-space distributions, Phys. Rev. A **31**, 1695 (1985).

[36] L. Yang, A. Karandikar, and R. Boehler, Flash heating in the diamond cell: melting curve of rhenium, Rev. Sci. Instrum. **83**, 063905 (2012).

[37] L. Burakovsky, N. Burakovsky, D. Preston, and S. Simak, Systematics of the third row transition metal melting: the HCP metals rhenium and osmium, Crystals **8**, 243 (2018).

[38] S. P. Ong, W. D. Richards, A. Jain, G. Hautier, M. Kocher, S. Cholia, D. Gunter, V. L. Chevrier, K. A. Persson, and G. Ceder, Python materials genomics (pymatgen): a robust, open-source python library for materials analysis, Comput. Mater. Sci. **68**, 314 (2013).

[39] B. J. Morgan, Vasppy: A Python suite for manipulating VASP input and output, Zenodo (2021), doi:10.5281/zenodo.4460130.

[40] N. Yasui, M. Sougawa, M. Hirai, K. Yamamoto, T. Okada, D. Yamazaki, Y. Kojima, H. Ohfuji, S. Kunitsugu, and K. Takarabe, High-Pressure and high-temperature synthesis of rhenium carbide using rhenium and nanoscale amorphous two-dimensional carbon nitride, Cogent Phys. **2**, 1076702 (2015).

[41] E. A. Juarez-Arellano, B. Winkler, A. Friedrich, L. Bayarjargal, V. Milman, J. Yan, and S. M. Clark, Stability field of the high-(P, T) Re_2C phase and properties of an analogous osmium carbide phase, J. Alloys Compd. **481**, 577 (2009).

[42] D. L. Perry and S. L. Phillips, *Handbook of Inorganic Compounds*, 2nd ed. (Taylor & Francis Group, Boca Raton, 2011), pp. 344–345.

[43] K. Momma and F. Izumi, VESTA 3 for three-dimensional visualization of crystal, volumetric and morphology data, J. Appl. Crystallogr. **44**, 1272 (2011).

[44] A. Magneli, S. Siitonen, B. Skrifvars, J. Schliack, and L. Reio, Studies on rhenium oxides, Acta Chem. Scand **11**, 28 (1957).

[45] B. Krebs, A. Mueller, and H. H. Beyer, Crystal structure of rhenium(VII) oxide, Inorg. Chem. **8**, 436 (1969).

[46] J.-E. Jørgensen, J. D. Jorgensen, B. Batlogg, J. P. Remeika, and J. D. Axe, Order parameter and critical exponent for the pressure-induced phase transitions in ReO_3, Phys. Rev. B **33**, 4793 (1986).

[47] K. Koumpouras and J. A. Larsson, Distinguishing between chemical bonding and physical binding using electron localization function (ELF), J. Phys.: Condens. Matter **32**, 315502 (2020).

[48] J. Shi, Z. Liang, J. Wang, S. Pan, C. Ding, Y. Wang, H.-T. Wang, D. Xing, and J. Sun, Double-Shock compression pathways from diamond to BC8 carbon, Phys. Rev. Lett. **131**, 146101 (2023).